The Journal of Experimental Biology 207, 3055-3066
Published by The Company of Biologists 2004
doi:10.1242/jeb.01141

Functional roles of the transverse and longitudinal flagella in the swimming motility of *Prorocentrum minimum* (Dinophyceae)

Iku Miyasaka*, Kenji Nanba, Ken Furuya, Yoshihachiro Nimura and Akira Azuma

Department of Aquatic Bioscience, Graduate School of Agricultural and Life Sciences, The University of Tokyo, 1-1-1 Yayoi, Bunkyo-ku, Tokyo 113-8657, Japan

*Author for correspondence (e-mail: miyasaka@aujaghi.fs.a.u-tokyo.ac.jp)

Accepted 14 June 2004

Summary

Equations describing the motion of the dinoflagellate *Prorocentrum minimum*, which has both a longitudinal and a transverse flagellum, were formulated and examined using numerical calculations based on hydrodynamic resistive force theory. The calculations revealed that each flagellum has its own function in cell locomotion. The transverse flagellum works as a propelling device that provides the main driving force or thrust to move the cell along the longitudinal axis of its helical swimming path. The longitudinal flagellum works as a rudder, giving a lateral force to the cell in a direction perpendicular to the longitudinal axis of the helix. Combining these functions results a helical swimming motion similar to the observed motion. Flagellar hairs present on the transverse flagellum are necessary to make the calculated cell motion agree with the observed cell motion.

Key words: *Prorocentrum minimum*, flagella, hydrodynamic resistive force theory, swimming, dinoflagellate.

Introduction

Dinoflagellates are microorganisms that swim using two flagella: a transverse flagellum encircling the cellular antero-posterior axis and a longitudinal one running posteriorly. There are numerous reports about diurnal vertical migration of dinoflagellates and their survival strategy is deeply linked to their swimming motion (Ault, 2000; Eppley et al., 1968; Franks, 1997; Horstmann, 1980; Kamykowski, 1981; MacIntyre et al., 1997; Olli et al., 1997; Olsson and Granéli, 1991). It has conventionally been thought that the forward thrust for swimming is provided by the transverse flagellum and/or the longitudinal flagellum, that the transverse flagellum produces cell rotation and that the longitudinal flagellum controls cell orientation. These suggestions are confirmed by observations of water movement around the organism (Jahn et al., 1963; Peters, 1929). Further electron microscopic studies (Honsell and Talarico, 1985) gave rise to hypothesizes of mechanisms how a transverse flagellum generates thrust (Gaines and Taylor, 1985; LeBlond and Taylor, 1976; for reviews, see Levandowsky and Kaneta, 1987; Sleigh, 1991; Goldstein, 1992). However, a quantitative examination of how the swimming motion and flagellar motion are linked is lacking, which makes it difficult to decide which flagellum is responsible for thrust generation during swimming. To answer the question, it is necessary to quantify the forces and moments generated by each flagellum and to relate them to the swimming speed, rotational speed, swimming trajectory and other swimming variables.

In a previous study (Miyasaka et al., 1998), the motility of *Prorocentrum minimum* (Fig. 1A) was investigated. Briefly, *P. minimum* was found to swim along a helical trajectory with the same side of the cell always facing the axis of the trajectory as, for example, lunar motion with respect to the Earth (Fig. 1B). Net swimming speed was 95.3 μm and the Reynolds number of the motion was 1.1×10^{-3}. The transverse flagellum encircles the anterior end of the cell, and a helical wave is propagated along it (Fig. 1A,E); this helical wave shows different half-pitches between the nearer and farther parts relative to the cellular antero-posterior axis (Fig. 1D). The longitudinal flagellum produces a planar sinusoidal wave propagated posteriorly (Fig. 1C).

In the present study, equations to describe the steady swimming motion of *P. minimum* based on resistive force theory (Gray and Hancock, 1955) are presented and the roles of both flagella are elucidated from the resulting calculations.

Materials and methods

The coordinate systems

A cell of *Prorocentrum minimum* (Pavillard) Schiller is here represented as a sphere of equivalent volume, moving steadily along a helical trajectory, with the variables describing the cell motion at first treated as unknowns. Two Cartesian coordinate systems or frames are established; one is the ‘inertial frame’ (X_I,Y_I,Z_I), fixed relative to the laboratory, and the other is the

'cell frame' (x,y,z), fixed relative to the cell. When the cell moves along a helical trajectory, the position of the cell $\boldsymbol{R}_c$ in the inertial frame is written in the inertial frame as:

$$\boldsymbol{R}_c = (V_X t,\ R_P \cos\Omega_c t,\ R_P \sin\Omega_c t)^T , \quad (1)$$

where V_X is net displacement speed, Ω_c is the angular speed of cell revolution, R_P the radius of the path helix and t is time, and superscript T indicates the transposed vector. The transformation to the cell frame from the inertial frame is performed by successive transformations using the Eulerian angles ψ, Θ and Φ describing cell orientation (Fig. 2A,B).

The transformation from the inertial frame (X_I,Y_I,Z_I), to the first frame (X',Y',Z'), is performed using a matrix $\boldsymbol{T}_1$, describing the rotation about the X_1 axis at the angular speed Ω_c as:

$$(X',Y',Z')^T = \boldsymbol{R}_c + \boldsymbol{T}_1 \cdot (X_I,Y_I,Z_I)^T , \quad (2)$$

where

$$\boldsymbol{T}_1 = \begin{pmatrix} 1 & 0 & 0 \\ 0 & \cos\Omega_c t & \sin\Omega_c t \\ 0 & -\sin\Omega_c t & \cos\Omega_c t \end{pmatrix} . \quad (3)$$

The transformation from the first frame, (X',Y',Z'), to the second frame, (X'',Y'',Z''), is performed using a matrix $\boldsymbol{T}_2$, describing the orientation ψ of the cell about the Z' axis as:

$$(X'',Y'',Z'')^T = \boldsymbol{T}_2 \cdot (X',Y',Z')^T , \quad (4)$$

where

$$\boldsymbol{T}_2 = \begin{pmatrix} \cos\Psi & \sin\Psi & 0 \\ -\sin\Psi & \cos\Psi & 0 \\ 0 & 0 & 1 \end{pmatrix} . \quad (5)$$

The transformation from the second frame (X'',Y'',Z''), to the third frame (X''',Y''',Z'''), is performed using a matrix $\boldsymbol{T}_3$, describing the orientation Θ, of the cell about the Y'' axis as:

$$(X''',Y''',Z''')^T = \boldsymbol{T}_3 \cdot (X'',Y'',Z'') , \quad (6)$$

where

$$\boldsymbol{T}_3 = \begin{pmatrix} \cos\Theta & 0 & -\sin\Theta \\ 0 & 1 & 0 \\ \sin\Theta & 0 & \cos\Theta \end{pmatrix} . \quad (7)$$

The transformation from the third frame (X''',Y''',Z'''), to the cell frame (x,y,z), is performed using the matrix $\boldsymbol{T}_4$, describing the orientation Φ, of the cell about the X''' axis as:

$$(x,y,z)^T = \boldsymbol{T}_4 \cdot (X''',Y''',Z''')^T , \quad (8)$$

where

$$\boldsymbol{T}_4 = \begin{pmatrix} 1 & 0 & 0 \\ 0 & \cos\Phi & \sin\Phi \\ 0 & -\sin\Phi & \cos\Phi \end{pmatrix} . \quad (9)$$

Therefore, the transformation from the inertial frame (X_I,Y_I,Z_I), to the cell frame (x,y,z), is performed as:

$$(x,y,z)^T = \boldsymbol{T}_4 \cdot \boldsymbol{T}_3 \cdot \boldsymbol{T}_2 \cdot [\boldsymbol{R}_c + \boldsymbol{T}_1 \cdot (X_I,Y_I,Z_I)^T] . \quad (10)$$

The unit direction vectors relative to the swimming trajectory $\boldsymbol{e}_{para}$, $\boldsymbol{e}_{rad}$ and $\boldsymbol{e}_{tan}$, (Fig. 2A) are defined as:

$$(\boldsymbol{e}_{para},\ \boldsymbol{e}_{rad},\ \boldsymbol{e}_{tan})^T = \boldsymbol{T}_1 \cdot (\boldsymbol{e}_{X_I},\ \boldsymbol{e}_{Y_I},\ \boldsymbol{e}_{Z_I})^T , \quad (11)$$

where $\boldsymbol{e}_{para}$ is parallel to the axis of the cylinder, $\boldsymbol{e}_{rad}$ is radial to a circular transections of the cylinder and $\boldsymbol{e}_{tan}$ is tangential to the circular transection and perpendicular to the cylinder's axis.

The swimming velocity $\mathbf{v}_c$, and rotational velocity $\boldsymbol{\omega}_c$, in the cell frame are transformed from those in the inertial frame as:

$$\mathbf{v}_c = (v_x,v_y,v_z)^T = \boldsymbol{T}_4 \cdot \boldsymbol{T}_3 \cdot \boldsymbol{T}_2 \cdot \boldsymbol{T}_1 \cdot (d\boldsymbol{R}_c/dt) , \quad (12)$$

and

$$\boldsymbol{\omega}_c = (\omega_x,\omega_y,\omega_z)^T \quad (13)$$

so that

$$\boldsymbol{\omega}_c = \boldsymbol{T}_4 \cdot \boldsymbol{T}_3 \cdot \boldsymbol{T}_2 \cdot \boldsymbol{T}_1 \cdot \begin{pmatrix} \Omega_c \\ 0 \\ 0 \end{pmatrix} + \boldsymbol{T}_4 \cdot \boldsymbol{T}_3 \cdot \boldsymbol{T}_2 \cdot \begin{pmatrix} 0 \\ 0 \\ \dot{\Psi} \end{pmatrix} + \boldsymbol{T}_4 \cdot \boldsymbol{T}_3 \begin{pmatrix} 0 \\ \dot{\Theta} \\ 0 \end{pmatrix} + \boldsymbol{T}_4 \cdot \begin{pmatrix} \dot{\Phi} \\ 0 \\ 0 \end{pmatrix} . \quad (14)$$

Upper dots in $\dot{\Psi}$, $\dot{\Theta}$ and $\dot{\Phi}$ and indicate time derivatives. Time derivatives of the Eulerian angles, $\dot{\Psi}$, $\dot{\Theta}$ and $\dot{\Phi}$, are assumed to be negligible compared with Ω_c, because *P. minimum* cells are observed to swim steadily along a helical trajectory with the same side always facing the trajectory axis (Fig. 1B).

Formulae for the flagella

The flagellar waves of the transverse and longitudinal flagella (Fig. 1A,B) are reconstructed as modified helical and sinusoidal waves, respectively (Figs 2C, 3), using variables from Miyasaka et al. (1998). Flagellar motion is formulated in the cell frame. The coordinate's origin is fixed at the cell's centre.

The cell's anterior end is represented by the intersection of the spherical cell and x axis; the valval suture plane is represented by plane x,y (Fig. 2C). While the basal parts of both flagella in the observed cell are attached to the anterior end of the cell, they are not included here in the flagellar model because their effects on the motion of the cell are thought to be small.

Transverse flagellum

The transverse flagellum encircles the anterior end of the cell and beats in a helical wave. It has two different pitches depending on the distance from the cellular antero-posterior axis (Fig. 1C–E; Miyasaka et al., 1998). The waveform is formulated here as a helical wave whose axis is a baseline circle of $[x_{bt},\ r_t\cos(s_t/r_t),\ r_t\sin(s_t/r_t)]^T$ ($0 \leqslant s_t \leqslant 2\pi r_t$), where x_{bt} and r_t are the x coordinates and the radius of the circle, respectively. The coordinate of a point on the transverse flagellum $r_t(s,t)$ is formulated as:

$$0 \leqslant s_t \leqslant n_t\lambda_t ,$$

$$r_t(s_t,t) = \begin{pmatrix} x_{bt} \\ 0 \\ 0 \end{pmatrix} + \begin{pmatrix} a_t \cos\varphi \\ (r_t + a_t \sin\varphi)\cos(s_t/r_t) \\ (r_t + a_t \sin\varphi)\sin(s_t/r_t) \end{pmatrix} , \quad (15)$$

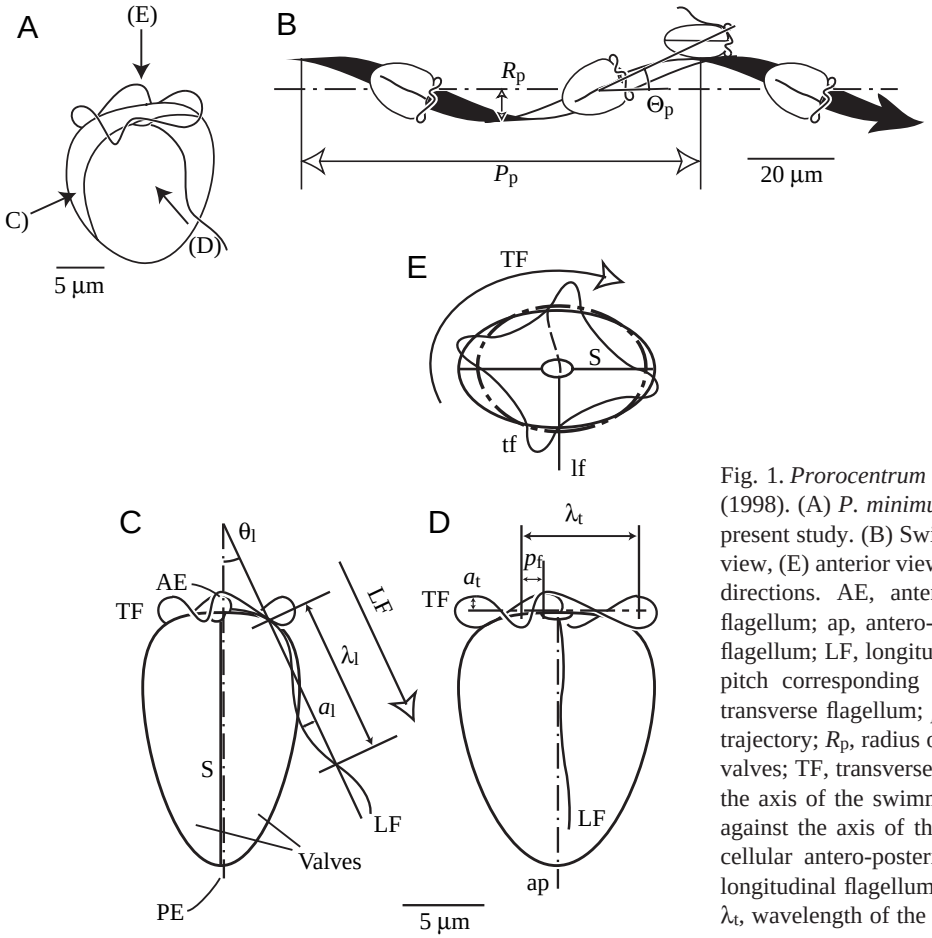

Fig. 1. *Prorocentrum minimum* motility described in Miyasaka et al. (1998). (A) *P. minimum* cell and directional terminology used in the present study. (B) Swimming trajectory. (C) Sutural view, (D) valval view, (E) anterior view, as indicated in A. Open arrows indicate wave directions. AE, anterior end; a_1, amplitude of the longitudinal flagellum; ap, antero-posterior axis; a_t, amplitude of the transverse flagellum; LF, longitudinal flagellum; PE, posterior end; p_n, the half-pitch corresponding to the adjacent parts to the ap axis of the transverse flagellum; p_f, remote part; P_p, pitch of helical swimming trajectory; R_p, radius of helical swimming trajectory; S, suture of two valves; TF, transverse flagellum; Θ the pitch angle of the cell against the axis of the swimming trajectory; Θ_p, the pitch angle of the cell against the axis of the swimming trajectory; θ_1, angle between the cellular antero-posterior axis and the center line of oscillation of longitudinal flagellum; λ_1, wavelength of the longitudinal flagellum; λ_t, wavelength of the transverse flagellum.

where s_t is the length along the axis of the helix, a_t is the amplitude, λ_t wavelength and n_t wavenumber of the helical wave, respectively (Fig. 2C). φ indicates the phase of this wave and two different pitches of the flagellum are expressed by the two alternative equations described below. $\varphi_0(s_t,t)$ is a non-negative real number and:

$$\varphi_0(s_t,t) = 2\pi(f_t t - s_t/\lambda_t)\mathrm{mod}(2\pi)\ , \qquad (16)$$

where f_t is the frequency of the helical wave. Therefore, when s and t vary, φ_0 varies within the range $0 \leqslant \varphi_0 < 2\pi$. φ switches as when $0 \leqslant \varphi_0 < 2\pi p$:

$$\varphi = \varphi_1 = \frac{\varphi_0}{2p}\ , \qquad (17)$$

as when $2\pi p \leqslant \varphi_0 < 2\pi$:

$$\varphi = \varphi_2 = \frac{\varphi_0 - 2\pi}{2(1-p)}\ , \qquad (18)$$

where p is the ratio of a part corresponding to the remote part, p_f, from the antero-posterior axis of the cell to the wavelength of the flagellum, λ_t, or p_f/λ_t (Fig. 1D) and ranges as $0<p<1$. φ_1 and φ_2 indicate equations for φ in two ranges. As $2\pi(f_t t - s_t/\lambda_t)$ increases, φ_0 changes in a saw-tooth-shaped wave with a period of 2π, and φ shows a saw-tooth-shaped wave with inclinations of $1/(2p)$ and $1/(2-2p)$ when $\varphi=\varphi_1$ and $\varphi=\varphi_2$, respectively (Fig. 3A). When φ changes as described above, $\cos\varphi$ alternates between two pitches in the ratio $p(1-p)$, as observed in the transverse flagellum in side view (Figs 1D, 3B).

When time t advances, the wave is propagated along the transverse flagellum, and the flagellar segments move along a circular trajectory in the plane of $z\cos(s_t/r_t) - y\sin(s_t/r_t) = 0$. The transverse flagellum is assumed to encircle completely the cellular antero-posterior axis (see Fig. 2C).

Longitudinal flagellum

The longitudinal flagellum moves as a wave in a plane perpendicular to the valval suture plane (Fig. 1C). The waveform is a sinusoidal wave in the xy plane whose centre line (Fig. 2C) is:

$$\begin{pmatrix} x_{bl} \\ y_{bl} \\ 0 \end{pmatrix} + \begin{pmatrix} s_1\cos\theta_1 \\ s_1\sin\theta_1 \\ 0 \end{pmatrix}\ , \qquad (19)$$

where x_{bl} and y_{bl} are the x and y coordinates of the point on this line where $s_1=0$. A point, $r_1(s_1,t)$, on the waveform is formulated as:

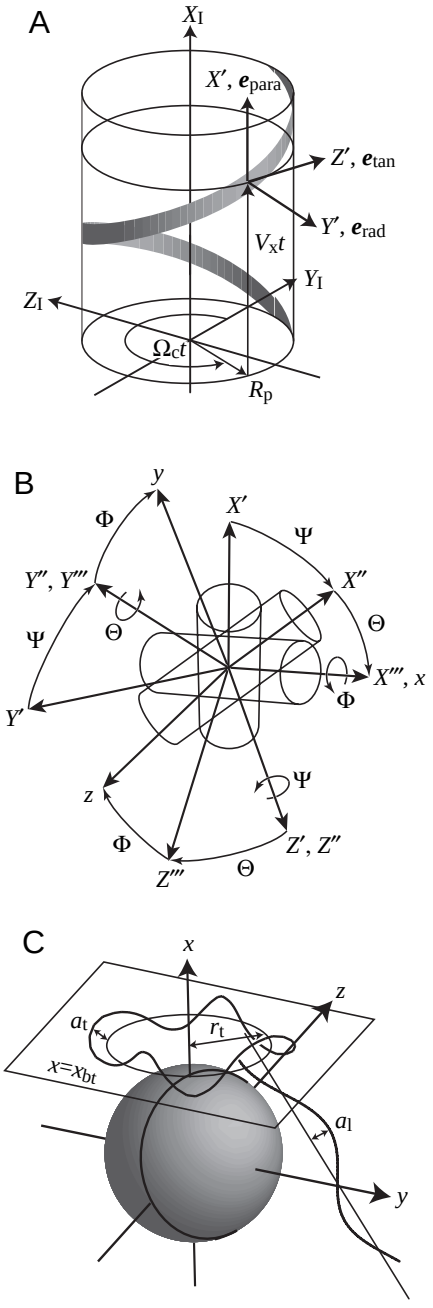

Fig. 2. Illustration of the coordinate systems and their transformation. (A) The helical swimming trajectory is shown on a cylinder. V_X is the net displacement speed of the cell, where Ω_c is the angular speed of the cell, R_p is the radius of the cylinder and t is time. $\boldsymbol{e}_{para}$, $\boldsymbol{e}_{tan}$ and $\boldsymbol{e}_{rad}$ are the unit direction vectors where $\boldsymbol{e}_{para}$ is parallel to the axis of the cylinder, $\boldsymbol{e}_{rad}$ is radial to a circular transections of the cylinder and $\boldsymbol{e}_{tan}$ is tangential to the circular transection whose plane is perpendicular to the cylinder's axis. (X_I,Y_I,Z_I) is the inertial frame fixed relative to the laboratory and (X',Y',Z') is a coordinate translating with the cell and rotating with the cell and is rotating about X' axis (identical to X_I axis) at the angular speed of Ω_c. $\boldsymbol{e}_{para}$, $\boldsymbol{e}_{tan}$ and $\boldsymbol{e}_{rad}$ are the components parallel to the net displacement, tangential and radial to the swimming trajectory. $(X',Y',Z')^T=\boldsymbol{R}_c+\boldsymbol{T}_1\cdot(X_I,Y_I,Z_I)^T$, where superscript T indicates the transposed vector, $\boldsymbol{R}_c$ is the position of the cell in the inertial frame (see Equation 1) and $\boldsymbol{T}_1$ is a matrix indicating the rotational movement of the cell defined in Equation 3, respectively. (B) Transformations between the coordinates $(X',Y',Z')^T \underset{\rightarrow}{T_2}(X'',Y'',Z'')^T \underset{\rightarrow}{T_3}(X''',Y''',Z''')^T \underset{\rightarrow}{T_4}(x,y,z)^T$, where Ω, Θ and Φ are the Eulerian angles indicating cell orientation and T_2–T_4 are defined in Equations 4–7, to define the cell frame (x,y,z). (C) Model of the *P. minimum* cell and flagella in the cell frame. a_1, amplitude of longitudinal wave; a_t, amplitude of transverse wave; r_t radius of the circle along which the transverse wave is propagating; x_{bt}, x coordinate of the circle along which the transverse wave is propagating.

$$0 \leqslant s_1 \leqslant n_1\lambda_1 ,$$

$$r_1(s_1,t) = \begin{pmatrix} x_{bl} \\ y_{bl} \\ 0 \end{pmatrix} + \begin{pmatrix} \cos\theta_1 & -\sin\theta_1 & 0 \\ \sin\theta_1 & \cos\theta_1 & 0 \\ 0 & 0 & 1 \end{pmatrix} \begin{pmatrix} s_1 \\ a_1 \cos 2\pi(f_1 t - s_1/\lambda_1) \\ 0 \end{pmatrix}, \quad (20)$$

where s_1 is the length of the line along which the flagellum wave propagates, $r_1(s_1,t)$ are coordinates of a point on the wave, a_1 is amplitude, λ_1 wavelength, f_1 frequency and n_1 wavenumber of the flagellar wave, and θ_1 is the angle between the wave's centre line and cell's antero-posterior axis.

Forces and moments acting on the flagella

The hydrodynamic forces and moments acting on the flagella are given by hydrodynamic resistive force theory (Gray and Hancock, 1955). The thrust and moment generated by a flagellar segment are derived from its velocity relative to the fluid, resistive force coefficients associated with the fluid viscosity and the length of the flagellar segment (Gray and Hancock, 1955). The relative velocity is calculated using the Stokes' solution for the flow around a sphere (Jones et al., 1994) and the resistive force is calculated for various configurations and arrangements of flagellar appendages or hairs (Brennen, 1974; Gray and Hancock, 1955; Holwill and Sleigh, 1967; Lighthill, 1976).

Gray and Hancock (1955) formulated the hydrodynamic force $d\boldsymbol{F}_f^H$ generated by a flagellar element of length dl and having a relative velocity $\boldsymbol{V}$ to the fluid, as:

$$d\boldsymbol{F}_f^H = -C_N\boldsymbol{V}_N dl - C_T\boldsymbol{V}_T dl , \quad (21)$$

where $\boldsymbol{V}_N$ and $\boldsymbol{V}_T$ are the velocity components in the normal and tangential directions to the flagellar shaft, respectively. C_N and C_T are the drag coefficients in the normal and tangential directions to the flagellar shaft, respectively. They proposed that C_N and C_T for a smooth-surfaced flagellum were:

$$C_T = \frac{2\pi\mu}{\ln(4\lambda/d) - \frac{1}{2}} \quad (22)$$

and

$$C_N = \frac{4\pi\mu}{\ln(4\lambda/d) - \frac{1}{2}} , \quad (23)$$

respectively, where λ is the flagellar wavelength along the

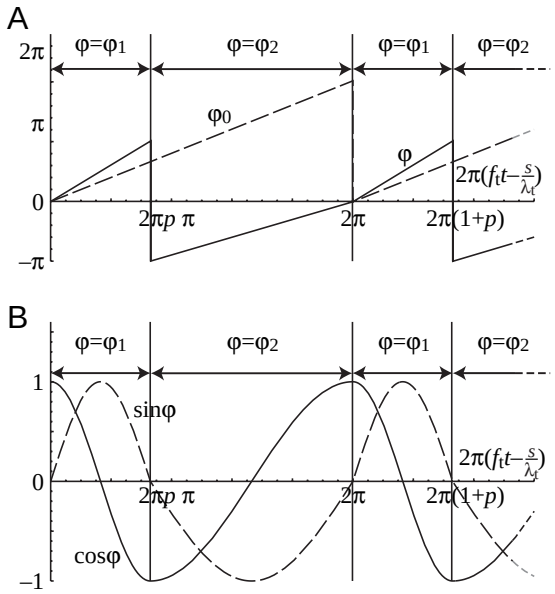

Fig. 3. Two-pitches model of the transverse flagellar wave. (A) φ_0 (broken line) and φ (solid line) which alternate between φ_1 and φ_2. (B) cosφ (solid line) and sinφ (broken line). φ indicates the phase of this wave and it switches between φ_1 and φ_2. $\varphi_1=\varphi_0/2p$ is the equation for φ when $0<\varphi_0<2\pi$, and $\varphi_2=(\varphi_0-2\pi)/2(1-p)$ is the equation for φ when $2\pi p''\varphi_0<2\pi$, where p is the ratio of a half pitch corresponding to the remote part of the antero-posterior axis of the cell to a wavelength and φ_0 is the minimum non-negative value for $2\pi(f_t t-s/\lambda_t)-2\pi m$, where t, s, f_t, λ_t and m are time, length along the circle where the transverse flagellum wave propagates, the frequency and wavelength of the helical wave and a positive integer that minimizes $\varphi_0(s,t)$, respectively.

flagellar shaft, d is the diameter of the flagellum and μ is the fluid viscosity. Lighthill (1976) improved these equations as:

$$C_T = \frac{2\pi\mu}{\ln(4\cdot 0.09\lambda/d)}, \tag{24}$$

and

$$C_N = \frac{4\pi\mu}{\ln(4\cdot 0.09\lambda/d)+\frac{1}{2}}. \tag{25}$$

Holwill and Sleigh (1967) investigated the hydrodynamics of a Chrosophyte flagellum, which has small thin rigid hairs attached perpendicularly to the flagellar shaft. They proposed that the C_N and C_T of such a hispid flagellum were given by the sum of the drag coefficients of the flagellar shaft and flagellar hairs:

$$C_N = C_N^f + n_{len}^h l^h \sum_{i=1}^{n_{sec}^h} (C_T^h \cos^2\theta_i + C_N^h \sin^2\theta_i), \tag{26}$$

and

$$C_T = C_T^f + n_{len}^h n_{sec}^h l^h C_N^h, \tag{27}$$

respectively, where l_h is the length of flagellar hairs, n_{sec} is the number of rows of flagellar hairs in cross section, n_{len} is the number of rows of flagellar hairs per unit length of flagellum, and θ_i is the angle between the moving direction of the flagellar shaft and the ith flagellar hair. Superscripts f and h indicate the flagellum and flagellar hairs, respectively. The drag coefficients C_N^f, C_T^f, C_T^f and C_N^f are derived from Equations 24 and 25 using the dimensions of the flagellar shaft and hairs. The alignment of the flagellar hairs has not been observed because they do not remain after fixation for electron microscopy. Holwill and Sleigh (1967) hypothesised two types of hispid flagellum having two and nine rows of flagellar hairs, or $n_{sec}^h=2$ and $n_{sec}^h=9$ in Equations 26 and 27. The $n_{sec}^h=2$ flagellum is hypothesised to have two rows of flagellar hairs on the opposite side of the flagellar shaft. The $n_{sec}^h=9$ flagellum is hypothesised to have nine rows, based on the idea that the alignment of the hairs corresponds to that of the nine microtubule pairs in the flagellar shaft.

In the present model, C_N and C_T are obtained from Lighthill (1976) and Holwill and Sleigh (1967), and the wavelength for each flagellum is calculated from Equations 15–20. The dimensions of the flagella and flagellar hairs were measured from electron micrographs of *P. minimum* in Honsell and Talarico (1985), which shows a smooth-surfaced longitudinal flagellum and a transverse flagellum with flagellar hairs. The longitudinal flagellum (LF) is regarded as smooth-surfaced with a diameter of 0.4 μm. Three types of transverse flagellum have been assumed, to allow for testing of the effect of the existence of flagellar hairs and their alignment: smooth-surfaced without flagellar hairs (sTF), bearing hairs in two rows (h2TF) and bearing hairs in nine rows (h9TF), projected on the transverse flagellum. The diameter of the transverse flagellum and the length and diameter of a flagellar hair are assumed to be 0.2 μm, 0.8 μm and 0.06 μm, respectively. The density of the flagellar hairs on the transverse flagellum is assumed to be eight hairs per micrometer, based on the electron micrographs in Honsell and Talarico (1985). The flagellar hairs on the transverse flagellum are assumed to be arranged at even angle intervals, and one of the flagellar hairs is assumed to be oriented in the direction of the movement relative to the cell frame. Therefore $\theta_i=2\pi(i-1)/n_{sec}^h$, where $i=1,2,\ldots n_{sec}^h$. The number of flagellar hairs around the flagellar transection n_{sec}^h was assumed to be two for h2TF and nine for h9TF.

The velocity of a flagellar element with reference to the cell frame $\mathbf{v}_{flag}$ is:

$$\mathbf{v}_{flag} = \frac{d\boldsymbol{r}}{dt}, \tag{28}$$

where $\boldsymbol{r}$ represents $\boldsymbol{r}_t(s_t,t)$ or $\boldsymbol{r}_1(s_1,t)$, with values taken from Miyasaka et al. (1998). The fluid velocity around the cell body is described by the Stokes' flow because of its small Reynolds number (Jones et al., 1994). When a sphere of radius r_c moves with a linear velocity of $\mathbf{v}_c$ and an angular velocity of ω_c, the flow due to the cell translation $\mathbf{v}_{tran}$ and rotation $\mathbf{v}_{rot}$, at point $\boldsymbol{r}$ in the cell frame according to Stokes' law is:

$$\mathbf{v}_{tran} = -\mathbf{v}_c\left(1-\frac{3r_c}{4r}-\frac{r_c^3}{4r^3}\right)+\frac{\mathbf{v}\cdot\boldsymbol{r}}{r^2}\boldsymbol{r}\,\frac{3r_c}{4r}\left(1-\frac{r_c^2}{r^2}\right) \tag{29}$$

and

$$\mathbf{v}_{rot} = \boldsymbol{\omega}_c \times \boldsymbol{r}\left(-1 + \frac{r_c^3}{r^3}\right), \quad (30)$$

respectively, where r is the distance from $\boldsymbol{r}$ to the origin of the cell frame, or the centre of the sphere (Lamb, 1932). The passive fluid velocities caused by the flagellar motion are assumed to be negligibly small in comparison with those caused by the cell motion, $\mathbf{v}_{tran}$ and $\mathbf{v}_{rot}$. Based on this assumption, the terms in Equation 21 are:

$$dl = \left|\frac{d\boldsymbol{r}}{ds}\right|, \quad (31)$$

$$\boldsymbol{V}_T = (\boldsymbol{V}\cdot\boldsymbol{e})\boldsymbol{e} \quad (32)$$

and

$$\boldsymbol{V}_N = \boldsymbol{V} - \boldsymbol{V}_T\ , \quad (33)$$

where s represents s_l or s_t. $\boldsymbol{e}$ indicates a unit tangential vector to the flagellar shaft as:

$$\boldsymbol{e} = d\boldsymbol{r}\,/\,dl\ , \quad (34)$$

and $\boldsymbol{V}$ indicates total velocity of flagellar element relative to the fluid as:

$$\boldsymbol{V} = (d\boldsymbol{r}/dt) + \boldsymbol{\omega}_c \times \boldsymbol{r} - \mathbf{v}_{tran} - \mathbf{v}_{rot}\ . \quad (35)$$

The force produced by the flagellar element is given by substitution of Equations 24–35 into Equation 21 and the moment $d\boldsymbol{M}_f^H$ generated by the element is given as:

$$d\boldsymbol{M}_f^H = \boldsymbol{r} \times d\boldsymbol{F}_f^H\ . \quad (36)$$

Inertial, buoyant and gravitational forces and moments acting on the flagella, and inertial force and moment acting on the added mass of flagella, are assumed to be negligibly small in comparison with those produced *via* hydrodynamic resistance.

Forces and moment acting on the cell

The forces and moments acting on the cell body arise from the inertia of the cell body, inertia of the added mass of the cell, hydrodynamic forces caused by the cell, gravity and the buoyancy of the cell. However, the Reynolds number of the swimming motion of the cell, which is 1.1×10^{-3}, shows that the hydrodynamic force and moment dominate the motion, and inertial forces and moments are negligibly small in comparison of hydrodynamic ones. The hydrodynamic drag force and moment are represented by the drag force $\boldsymbol{F}_c^H$ and moment $\boldsymbol{M}_c^H$ required by the hydrodynamic resistance to move a sphere of radius r_c at velocity $\mathbf{v}_c$ and rotational velocity $\boldsymbol{\omega}_c$ as:

$$\boldsymbol{F}_c^H = -6\pi\mu r_c\mathbf{v}_c\ , \quad (37)$$

and

$$\boldsymbol{M}_c^H = -8\pi\mu r_c^3\boldsymbol{\omega}_c\ , \quad (38)$$

respectively, where μ is the viscosity of the fluid. The force arising from gravity and buoyancy on the motion depends on the densities of the cell body and medium, which are 1.082×10^3 kg m^{-3} and 1.021×10^3 kg m^{-3}, respectively (Kamykowski et al., 1992). Gravitational and buoyant forces acting on the model cell are 8.23×10^{-12} N and 7.76×10^{-12} N, respectively, and their resultant force 4.7×10^{-13} N is much smaller than the hydrodynamic force acting on the cell moving in the fluid at the speed around 100 μm s^{-1}, which is in the region of 10^{-11} N. Gravitational and buoyant forces acting on the cell do not generate moment to rotate the cell body because the cell body is represented by a sphere with a homogeneous density.

Equations of motion

The equations of motion used to simulate steady motion of the cell can be written as:

$$\Sigma\int d\boldsymbol{F}_f^H + \boldsymbol{F}_c^H = 0\ , \quad (39)$$

and

$$\Sigma\int d\boldsymbol{M}_f^H + \boldsymbol{M}_c^H = 0\ , \quad (40)$$

where the inertial, gravitational and buoyant forces and moments are neglected and there are no other external forces and moments. Equations 39 and 40 are solved to find v_x, v_y, v_z, ω_x, ω_y an ω_z, and the hydrodynamic forces and moments generated by the flagella and acting on the cell are evaluated. Equations 12–14 are solved for variables describing the cell motility in the inertial frame V_X, Ω_c, R_p, ψ, Θ and Φ.

Using the acquired solutions, the power P done by the entire flagellum against the hydrodynamic force is given by integrating an inner product of flagellar velocity vector $\boldsymbol{V}$ and the hydrodynamic force $d\boldsymbol{F}_f^H$ as:

$$P = \int\boldsymbol{V}\cdot d\boldsymbol{F}_f^H\ . \quad (41)$$

The conversion efficiencies from the power done by flagellar movement against the hydrodynamic force to cell's motion are given by a ratio of a sum of power done by the flagellum (a) of the cell, ΣP. The efficiency of the flagellar motion into swimming and rotation is given as:

$$\eta = \frac{\mathbf{v}_c\cdot\boldsymbol{F}_c^H + \boldsymbol{\omega}_c\cdot\boldsymbol{M}_c^H}{\Sigma P}\ , \quad (42)$$

where $\mathbf{v}_c\cdot\boldsymbol{F}_c^H$ and $\boldsymbol{\omega}_c\cdot\boldsymbol{M}_c^H$ are the hydrodynamic power for motion and rotation of the cell, respectively. Efficiency for the cell's swimming along the swimming path η_{path} and for its net travelling along a linear distance η_{linear} are given as:

$$\eta_{path} = \frac{\mathbf{v}_c\cdot\boldsymbol{F}_c^H}{\Sigma P} \quad (43)$$

and

$$\eta_{linear} = \frac{\mathbf{v}_{para}\cdot\boldsymbol{F}_c^H}{\Sigma P}\ , \quad (44)$$

respectively, where $\mathbf{v}_{para}$ is the component of $\mathbf{v}_c$ in the direction of $\boldsymbol{e}_{para}$.

Model simulations

Seven model cells are considered in simulation: a cell with a longitudinal flagellum (LF), with a hispid transverse

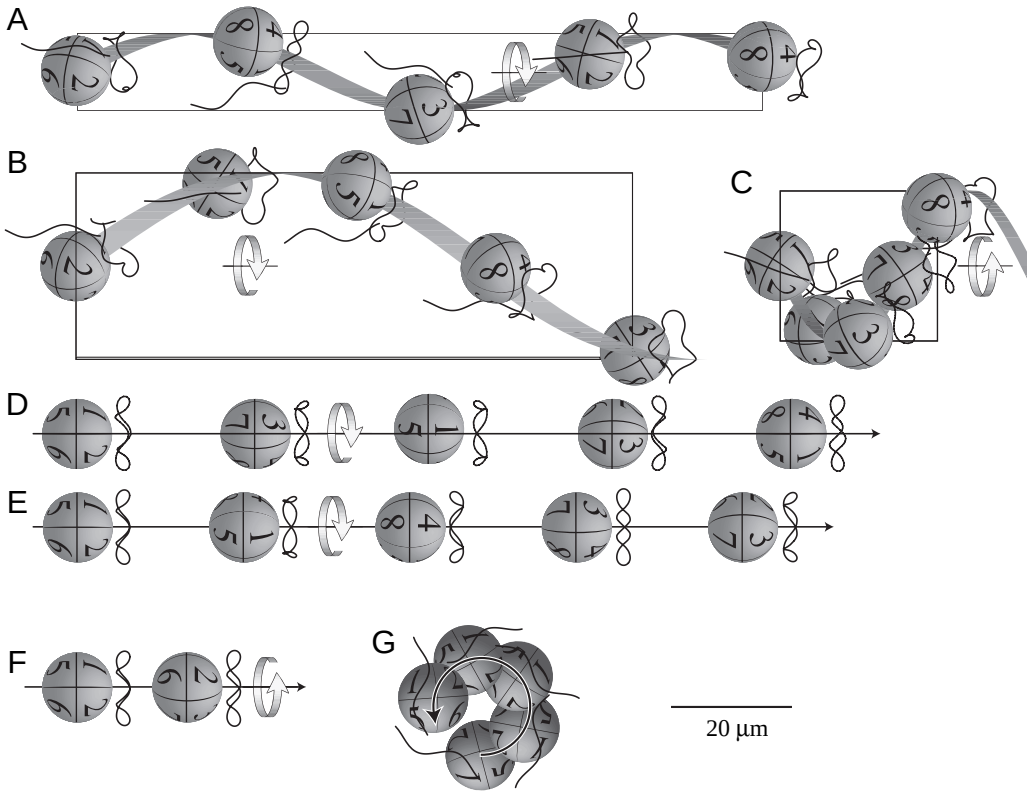

Fig. 4. Schematic illustrations of the movement of the model cell (Table 1). Cell motility variables and abbreviations are given in Table 1. The cells are viewed along the Y_I axis except in G, which is viewed along the X_I axis (see Fig. 2). The position and orientation of the cell is shown at intervals of 0.25 s, except F, where the time interval is 1 s. The spheres representing cells are divided into eight regions labelled (from left to right) 1–4 and 5–8 on the upper and lower hemispheres, respectively. Arrows indicate the swimming trajectory and direction of turning. (A) LF+h2TF, (B) LF+h9TF, (C) LF+Stf, (D) h2TF, (E) h9TF, (F) Stf, (G) LF.

Table 1. *Motilities of model* P. minimum *cells with various flagellar compositions*

	Observed cell (N=7)*	Model cells						
	LF+hTF	LF+h2TF	LF+h9TF	LF+sTF	h2TF	h9TF	sTF	LF
$\|\mathbf{v}_c\|$ (μm s^{-1})	107.7±54.6	129.4	118.9	55.8	118.1	110.0	18.2	36.4
V_X (μm s^{-1})	95.3±46.0	113.4	92.2	26.2	118.1	110.0	18.2	0
Ω_c (rad s^{-1})	7.04±1.45	9.05	4.27	–4.02	10.0	4.34	–4.78	4.52
R_P (μm)	7.49±2.33	6.4	15.5	12.5	0	0	0	1.54
Ψ (rad)		–0.26	–0.34	–0.37	0	0	0	1.57
Θ (rad)	0.51±0.12	–0.21	–0.48	0.37	0	0	0	–0.39
Φ (rad)		2.7	2.4	3.1	0	0	0	1.57

$|\mathbf{v}_c|$, swimming speed along the trajectory; V_X, net displacement speed; Ω_c, angular speed; ψ, Θ, Φ, Eulerian angles indicating cell orientation; R_P, radius of helical swimming trajectory.

*Observed values are means ± S.D. from Miyasaka et al. (1998).

LF, longitudinal flagellum; TF, transverse flagellum; h2TF, transverse flagellum bearing hairs in two rows; h9TF, transverse flagellum bearing hairs in nine rows; sTF, smooth transverse flagellum (hairless).

flagellum (h2TF and h9TF), with a smooth transverse flagellum (sTF), with a longitudinal flagellum plus a hispid transverse flagellum (LF+h2TF and LF+h9TF) or with a longitudinal flagellum plus a smooth transverse flagellum (LF+sTF). Cells with a transverse flagellum are examined for changes in the ratio of swimming speed to wave propagation speed $V_X/f_t\lambda_t$, the ratio of rotational frequency to flagellar frequency Ω_c/f_t, and efficiency η, as a function of the amplitude-to-wavelength ratio $\pi a_t/\lambda_t$, to allow direct comparisons with data obtained for other flagellated organisms in previous studies (Chwang and Wu, 1971, 1974; Coakley and Holwill, 1972; Higdon, 1979; Holwill, 1966; Holwill and Burge, 1963; Holwill and Sleigh, 1967; Lighthill, 1976). All calculations were performed using a Macintosh G3 equipped with Mathematica version 4.1 (Wolfram Research, IL, USA).

Results

Movement of cells

The results of the calculations gave distinctively different movement patterns for each of the seven model cells (Table 1, Fig. 4). The traces of the swimming trajectories fall into three

Table 2. *Forces and moments generated by each flagellum in model cells*

Model cell	Flagellum	$\boldsymbol{F}_{para}$ (10^{-12} N)	$\boldsymbol{F}_{tan}$ (10^{-12} N)	$\boldsymbol{F}_{rad}$ (10^{-12} N)	$\boldsymbol{M}_{para}$ (10^{-17} Nm)	$\boldsymbol{M}_{tan}$ (10^{-17} Nm)	$\boldsymbol{M}_{rad}$ (10^{-17} Nm)
LF+h2TF	h2TF	11.7	1.6	–4.4	8.0	1.4	–2.1
	LF	0.51	4.7	4.4	–3.8	–1.4	2.1
LF+h9TF	h9TF	9.2	5.0	–4.0	2.6	1.8	–1.2
	LF	0.75	2.4	4.0	–0.58	–1.8	1.2
LF+sTF	sTF	1.0	0	0	–1.34	–1.0	0.39
	LF	1.8	5.0	0	–0.57	1.0	–0.39
h2TF	h2TF	12.7	0	0	5.17	0	0
h9TF	h9TF	11.2	0	0	2.0	0	0
sTF	sTF	1.97	0	0	–2.23	0	0
LF	LF	0	7.9	0	2.9	0	0

F and ***M*** indicate force and moment; subscripts para, tan and rad indicate components parallel, tangential and radial to the direction of net displacement, respectively.

See Table 1 for abbreviations pertaining to model cells and flagella.

types. Cells with both transverse and longitudinal flagella move along a helical trajectory. Those with a transverse flagellum swim along a linear trajectory and rotate at more than twice the speed of the corresponding cell with a longitudinal flagellum (Table 1, Fig. 4D–F). The LF cell swims along a circular trajectory, rotating sideways and making no net displacement (Fig. 4G).

Flagellar hairs on the transverse flagellum determined the direction of cell rotation and the speed of cell displacement and rotation. Cells that have hairs on the transverse flagellum rotated in a right-handed direction, i.e. in the same direction as the wave propagation of the transverse flagellum (Table 1, Fig. 4A,B,D,E), while cells LF+sTF and sTF rotated in a left-hand direction (Fig. 4C,F). Swimming speed decreased from h2TF, through h9TF and sTF for cells without a longitudinal flagellum. Addition of a longitudinal flagellum does not change the order. Cells with a larger value of C_T/C_N for the transverse flagellum swam faster (Table 1).

The force and moment vectors generated by each flagellum were also calculated and decomposed into the components in the $\boldsymbol{e}_{para}$, $\boldsymbol{e}_{rad}$ and $\boldsymbol{e}_{tan}$ directions (Fig. 2A and Equation 11), according to the thrust and moment function (Table 2). The transverse flagellum provided over 90% of the thrust force $\boldsymbol{F}_{para}$ to drive the cell, and all the longitudinal moment $\boldsymbol{M}_{para}$ to rotate the cell and the longitudinal flagellum in the LF+h2TF and LF+h9TF cells. While the contribution of the longitudinal flagellum to the thrust $\boldsymbol{F}_{para}$ was less than 10%, the flagellum generated the lateral force, $\boldsymbol{F}_{tan}$, to make the swimming trajectory helical. In cells with only a transverse flagellum (h2TF, h9TF and sTF cells), the flagellum did not generate $\boldsymbol{F}_{tan}$ (Table 2). In the LF cell, the longitudinal flagellum generated $\boldsymbol{F}_{tan}$ and $\boldsymbol{M}_{para}$ but no $\boldsymbol{F}_{para}$, and the cell swam along a circular path.

The net efficiencies η ranged from 2.3 to 7.3% among the seven model cells (Table 3). Comparison of η with the travelling efficiency η_{path} indicates a nearly one-third reduction in efficiency due to rotation in the h2TF and LF+h2TF cells. In the LF+sTF cell, the advancing efficiency η_{linear} is one-quarter of η_{path}, which is attributed a greater deviation from the travelling path. In the LF cell η_{linear} was zero because the cell swims along a circular trajectory without advancing.

Table 3. *Efficiency of model* P. minimum *cells with various flagellar compositions*

Efficiency	Model cell						
	LF+h2TF	LF+h9TF	LF+sTF	h2TF	h9TF	sTF	LF
η (%)	3.5	2.3	2.4	4.2	2.4	2.6	7.3
η_{path} (%)	2.9	2.1	1.9	3.0	2.2	0.7	5.2
η_{linear} (%)	2.2	1.4	0.5	3.0	2.2	0.7	0.0

η, net efficiency, is the efficiency of the transformation of flagellar hydrodynamic power to the cell's kinetic power composed of linear and rotational motions; η_{path}, travelling efficiency, is the efficiency of transformation flagellar hydrodynamic power to the cell's hydrodynamic power for travelling along the swimming path; η_{linear}, advancing efficiency, is the efficiency of the transformation of flagellar hydrodynamic power to the cell's hydrodynamic power for advancing a straight line along the central axis of helix.

See Table 1 for abbreviations pertaining to model cells.

Characterization of the transverse flagellum

The mechanism of thrust generation by the transverse flagellum, which is the main forward thrust generator (Table 2), was investigated and we describe the result of the simulation for the h2TF cell (Fig. 5A) as a simplest case.

The motion and thrust generation of a flagellar segment of a given unit length are described as follows. When a transverse flagellum propagates a quasi-helical wave around the cell body, the flagellar segment moves along a planar circular trajectory (Fig. 5A). The thrust vector generated by the flagellar segment depends on the phase of the wave. The integration of the thrust over a period gives forward thrust,

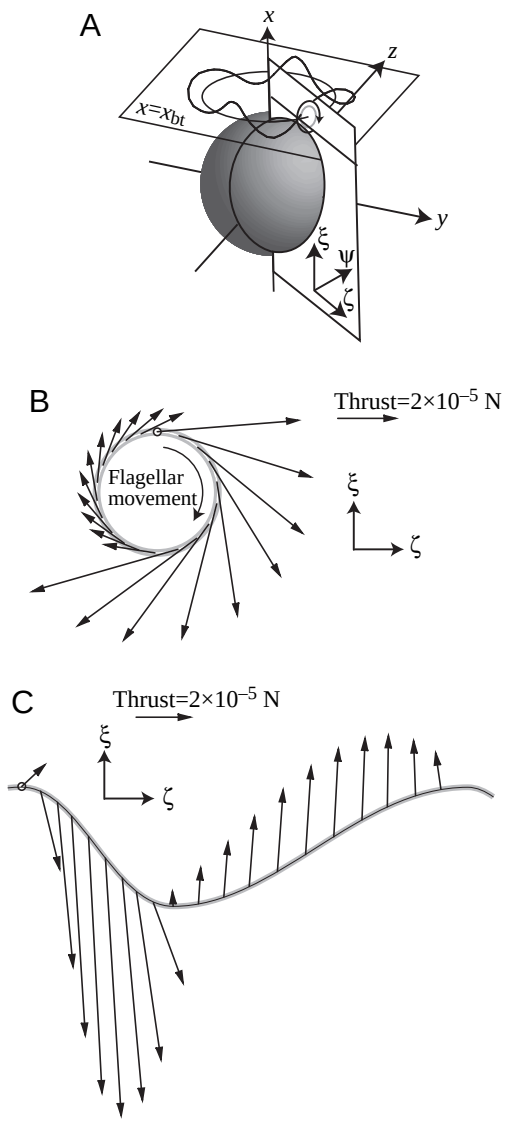

Fig. 5. Thrust made by flagellar shaft and flagellar hairs of the transverse flagellum in an hTF cell during a cycle of the transverse flagellum. Thick gray lines indicate the trajectory of a segment on the flagellum and the small arrows on the line indicate the direction and strength of the thrust. The change of force vectors are drawn at intervals of 1.4 ms. (A) hTF cell and flagellar trajectory's plane. Coordinate system ξ, ψ and ζ are set as ξ=*x*, and as the trajectory of the segment is included in ψ–ζ plane. (B) Flagellar movement and the generated force vectors in ξ–ψ plane. (C) Flagellar movement and the generated force vectors in ξ–ζ plane.

because the thrust strength is asymmetric between forward and backward directions (Fig. 5B,C). There are two reasons for this assmmetry. One is the Stokes' flow field caused by the cell translation and rotation. This attenuates the hydrodynamic force generated adjacently to the cell body. The hydrodynamic thrust force decreases in strength by the term containing $r_c/\boldsymbol{r}$ in Equations 29 and 30. The forward thrust is generated at a remote part of the cell surface and becomes larger than the backward thrust, which is generated at a nearby part of the cell. The second is the asymmetry of the waveform, introduced to the model by Equations 5 and 18. Because of this asymmetry, the thrust generated during the backward motion of the flagellar segment is larger than that of the forward motion (Fig. 5C). Therefore, the integrated hydrodynamic force in the direction *x* component results in a forward thrust in the hTF cell.

The component tangential to the baseline circle causes the moment around the cell's antero-posterior axis to rotate the cell (Fig. 5C); this and the radial component balance each other between the counterpart of the transverse flagellum. Simulations were made of the relationship between the wavenumber and the resultant thrust. When there are four waves in the transverse flagellum, the thrust and moment are constant because most of the force components in the radial direction counterbalance each other (Fig. 6A). While this does not change if the wavenumber is an odd number, it does change when the wavenumber is not an integer. The forward thrust generated by a transverse flagellum with wavenumbers of 3.5 and 4.5 oscillates, depending the phase of the wave (Fig. 6A). The forward thrust by a cell with a longitudinal flagellum also fluctuates. It fluctuates, however, when the wavenumber on the longitudinal flagellum is an integer (Fig. 6A). The fluctuation of the forward thrust by a cell with a longitudinal flagellum is apparently a result of the center line of the longitudinal flagellum not penetrating the center of the spherical cell (Fig. 6A). The ratio of fluctuation to the mean thrust of the longitudinal flagellum is larger than that of the transverse flagellum, i.e. the transverse flagellum provides a stable force and moment. This feature of the transverse flagellum is attributed to its radial symmetry around the cellular antero-posterior axis. This feature makes the transverse flagellum unable to generate a force to change the swimming direction of the cell. It is reasonable that the longitudinal flagellum works to change the cell orientation while the transverse flagellum is at rest (Miyasaka et al., 1998).

Simulations were made of the relationship between the wavelength and the resultant speed and rotational frequency. The speed ratio $V_X/(f_t\lambda_t)$, frequency ratio Ω_c/f_t and net efficiency η change as functions of $\pi a_t/\lambda_t$, in h2TF, h9TF and sTF cells (Fig. 7). The net efficiency η peaks at $\pi a_t/\lambda_t \cong 0.7$ in the h2TF cell and at $\pi a_t/\lambda_t \cong 1.0$ in h9TF and sTF cells (Fig. 7C).

Discussion

Waveforms of *P. minimum* flagella were formulated and examined by means of a numerical model based on the hydrodynamic resistive theory. The motility of the observed cells was reproduced by the LF+h2TF cell (Table 1, Fig. 4A), and this model proved to be a potent device for quantitatively treating the motility of *P. minimum*.

What are the functions of the two flagella in swimming? The results of the calculations lead to the following conclusions. In cells with only a transverse flagellum, the flagellum generates $\boldsymbol{F}_{para}$ and $\boldsymbol{M}_{para}$ (Table 2), and the cells swim along a straight line (Table 1, Fig. 4). In the LF cell, the flagellum generates

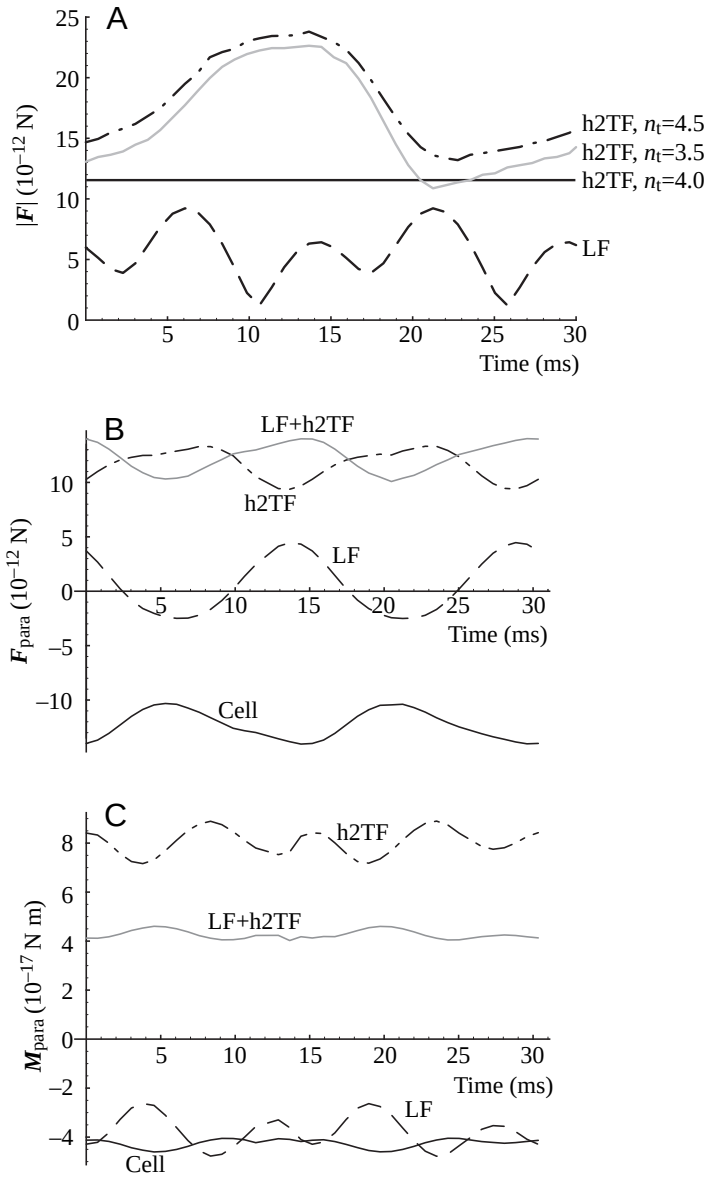

Fig. 6. Temporal changes in the forces and moments generated the flagellum and cell. (A) Temporal changes of the thrust resulting in net displacement $\boldsymbol{F}_{para}$ generated by various types of cells with a flagellum: as h2TF cell with a transverse flagellum of wavenumber of 4.5 (dot-dashed line), h2TF cell with a transverse flagellum of wavenumber of 3.5 (gray line), h2TF cell with a transverse flagellum of wavenumber of 4.0 (solid line) and LF cell with a longitudinal flagellum (broken line). (B) Temporal changes in force in the direction parallel to net displacement $\boldsymbol{F}_{para}$, in the hTF+LTF cell generated by the transverse flagellum (dot-dashed line), the longitudinal flagellum (broken line), sum of the two types of flagella (gray line) and drag force by the cell body (solid line). (C) Temporal changes in the moment around the antero-posterior axis of the cell $\boldsymbol{M}_{para}$, in the hTF+LTF cell generated by the transverse flagellum (dot-dashed line), the longitudinal flagellum (broken line), sum of the two types of flagella (gray line) and drag force by the cell body (solid line).

$\boldsymbol{F}_{tan}$ and $\boldsymbol{M}_{para}$, but no $\boldsymbol{F}_{para}$, and the cell makes no net displacement but rotates sideways (Fig. 4). While net efficiency η is highest for the LF cell among the model cells, the advancing efficiency η_{linear} is zero for this cell (Table 3). The motion of the LF+h2TF cell appears to be the sum of the two types described above: the transverse flagellum contributes 96% of $\boldsymbol{F}_{para}$ and all of $\boldsymbol{M}_{para}$, while the longitudinal flagellum generates 75% of $\boldsymbol{F}_{tan}$ (Table 2). The longitudinal flagellum of this cell generates negative $\boldsymbol{M}_{para}$ and 4% of $\boldsymbol{F}_{para}$, while that of the LF cell generates positive $\boldsymbol{M}_{para}$ and no $\boldsymbol{F}_{para}$. This indicates that the central line of the longitudinal flagellum is kept stable by its angle with the antero-posterior axis, and this stability enables the longitudinal flagellum to generate $\boldsymbol{F}_{para}$. The roles of the two flagella in LF+h9TF and LF+sTF cells can be explained similarly, while the motion of the LF+sTF cell (Fig. 6C) and its low travelling efficiency η_{linear} (Table 3) also resemble those of the LF cell because the sTF generates less force and moment than h2TF or h9TF does, allowing the properties of the longitudinal flagellum to dominate (Table 2). To summarise, the transverse flagellum provides thrust to move the cell along the longitudinal axis of the helical swimming path and rotates the cell about its antero-posterior axis. The longitudinal flagellum makes the swimming trajectory helical, and retards cell rotation.

For microorganisms, there are two advantages of active swimming over passive movement by gravity and buoyancy: faster movement and the ability to search for a more suitable place for survival. The former increases the rate of diffusion between the cell surface and the matrix fluid, by means of which it exchanges dissolved substances. For example, when a spherical microorganism with a diameter of 10 μm moves relative to the matrix fluid at speeds of 10 μm s^{-1} and 100 μm s^{-1}, the flux of dissolved substances across the cell surface increases by 2% and 40%, respectively, relative to a stationary cell (Lazier and Mann, 1989). A moving organism can also search for appropriate concentration gradients. For this purpose, a helical swimming path is more useful than a straight one in spite of the longer distance for the same displacement. This is because a helical swimming path enables detection of three-dimensional components of a gradient whereas a straight path allows detection of only one dimension (Crenshaw, 1996). For a *P. minimum* cell, the transverse flagellum enables the cell to achieve a high swimming speed. Addition of a longitudinal flagellum to the h2TF cell did not cause it to swim faster or more efficiently, as shown in smaller net displacement speed V_X, or lesser efficiencies (η, η_{path} and η_{linear}) in the LF+h2TF cell than in the h2TF cell (Tables 1, 3). The longitudinal flagellum, however, gives a cell the ability to search in the fluid, because it makes the swimming trajectory helical, allowing the cell to swim in a three-dimensional gradient and widening the fluid volume through which the cell passes. Turning the cell in a favourable direction also requires a longitudinal flagellum (Hand and Schmidt, 1975; Miyasaka et al., 1998).

How does the waveform of the transverse flagellum work in the observed cell motility? The net efficiency η reaches an optimum when $\pi a_t/\lambda_t \cong 0.7$ in the h2TF cell and $\pi a_t/\lambda_t \cong 1.0$ in

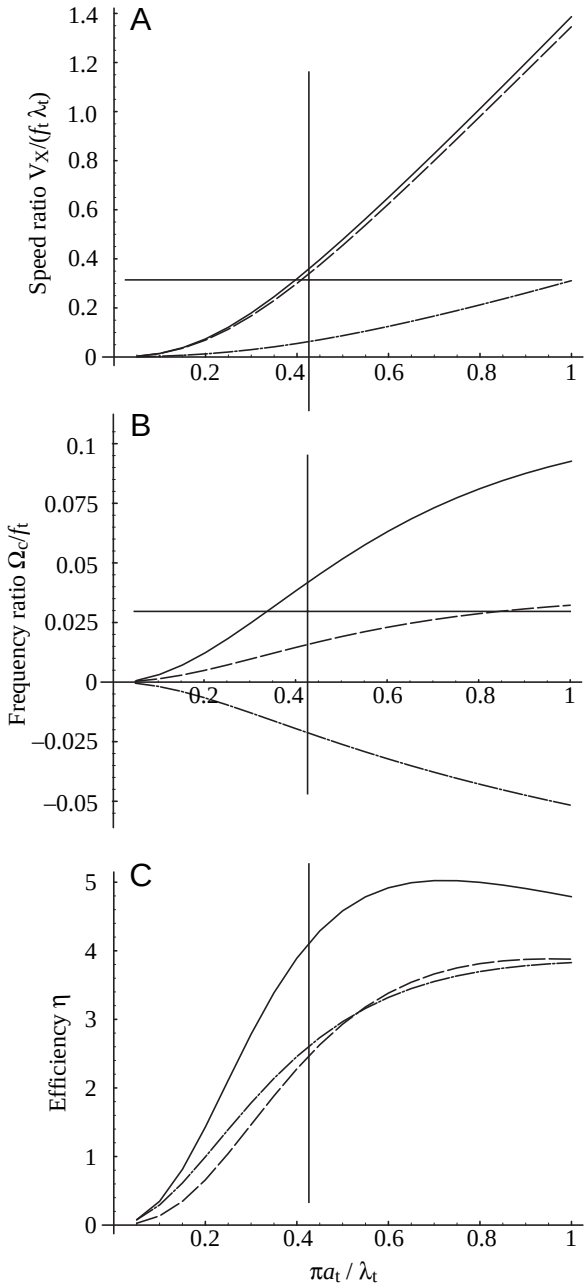

Fig. 7. The cell swimming motion as a function of the amplitude-to-wavelength ratio $\pi a_t/\lambda_t$ in model cells with a transverse flagellum. Solid, broken and dot-dashed lines indicate h2TF, h9TF and sTF cells, respectively. Horizontal and vertical lines show the average value for observed cells (Miyasaka et al., 1998; Table 1). (A) Speed ratio $V_X/(f_t\lambda_t)$. (B) Frequency ratio Ω_c. (C) Efficiency η. a_t, amplitude of transverse flagellum wave; λ_t, wavelength of transverse flagellum wave; V_X, net displacement speed of cell; f_t, frequency of transverse flagellum wave; Ω_c, angular speed of cell. See Table 1 for model cell abbreviations.

h9TF and sTF cells, respectively (Fig. 7). The amplitude-to-wavelength ratio $\pi a_t/\lambda_t$ for the optimum efficiency is larger than those found in past studies on flagella of spermatozoa or bacteria (Anderson, 1974; Holwill and Burge, 1963; Holwill and Peters, 1974; Holwill and Sleigh, 1967). This feature of the transverse flagellum is attributed to its position, which is so close to the cell surface that the contribution of the no-slip condition of the fluid caused by the Stokes' flow field is significant. When the model does not include the no-slip condition on the cell surface, as in the case of the flagellum being sufficiently remote from the cell surface, the resultant linear velocity is a half of the observed swimming speed. This suggests that the no-slip condition on the cell surface contributes to effective propulsion by the transverse flagellum.

Our results clearly demonstrate in terms of hydrodynamics that the existence of flagellar hairs on a transverse flagellum reverses the cell's rotational direction, as previously noted by Gaines and Taylor (1985). The smooth-surfaced transverse flagellum generates less thrust and moment than the observed cells (Table 1). The LF+h9TF cell has a smaller Ω_c than the actual cell, while the LF+h2TF cell has a Ω_c close to the real cells (Table 1). Although the arrangement of flagellar hairs in *P. minimum* has not yet been published, the simulations suggest that the transverse flagellum possesses flagellar hairs arranged to form two rows in a cross section of the flagellum projecting perpendicularly to the direction of the flagellar movement.

In conclusion, we propose the functions of the two flagella of *P. minimum* are as follows: the transverse flagellum acts as a propulsion device, to move the cell along the longitudinal axis of the helical swimming path and rotate it about its antero-posterior axis; the longitudinal flagellum acts as a rudder, to produce a helical swimming trajectory, and controls the orientation of the cell. Flagellar hairs on the transverse flagellum are probably present because they are necessary to produce simulated cell motion, in agreement with that observed in *P. minimum*. This is the first numerical evaluation of the functions of the transverse and longitudinal flagella of a dinoflagellate.

List of symbols and abbreviations

a_t	amplitude of the helix
C	drag coefficient
d	diameter of the flagellum
$\boldsymbol{e}_{para}$, $\boldsymbol{e}_{rad}$, $\boldsymbol{e}_{tan}$	unit direction vectors relative to the swimming trajectory
f (superscript)	flagellum hair
$\boldsymbol{F}$	force
f_1	frequency of the longitudinal flagellar wave
$\boldsymbol{F}_c^H$	drag force
$\boldsymbol{F}_f^H$	hydrodynamic force
f_t	frequency of the transverse helical wave
h (superscript)	flagellar hair
l	length
LF, l (subscript)	longitudinal flagellum
$\boldsymbol{M}$	moment
$\boldsymbol{M}_c^H$	drag moment
$\boldsymbol{M}_f^H$	moment generated by the flagellar element
n_1	wavenumber of the longitudinal flagellar wave
n_{len}	number of rows of the flagellar hair per unit length of flagellum

n_{sec}	number of rows of flagellar hairs in cross section
n_t	wavenumber of the transverse flagellar wave
P	power
p	ratio of a half pitch
r	radius
$\boldsymbol{r}$	position vector of a point on a flagellum
$\boldsymbol{R}_c$	position of the cell in the inertial frame
R_P	radius of the path helix
s_1	length along the axis of the longitudinal flagellar wave
s_t	length along the axis of the transverse flagellar wave
T (superscript)	transposed vector
$\boldsymbol{T}$	matrix
t (subscript)	transverse flagellum
t	time
TF	transverse flagellum
$\boldsymbol{V}$	relative velocity
$\mathbf{v}_c$	swimming velocity
$\mathbf{v}_{flag}$	velocity of a flagellar element
V_X	net displacement speed
X_I, Y_I, Z_I	Cartesian coordinates 'inertial frame'
x, y, z	Cartesian coordinates 'cell frame'
θ	angle between the wave's centre line and cell's antero-posterior axis
φ	phase of helical wave
η	swimming efficiency
ξ, ψ, ζ	coordinates
ψ, Θ, Φ	Eulerian angles describing cell orientation
Θ_P	pitch angle of the cell against the axis of the swimming trajectory
$\boldsymbol{\omega}_c$	rotational velocity
Ω_c	angular speed of cell revolution
η_{linear}	advancing efficiency
η_{path}	travelling efficiency
λ_t	wavelength of the helix
μ	fluid viscosity

The authors are grateful to anonymous referees for their helpful suggestions to an earlier version of this manuscript. We also thank Dr Y. Fukuyo for providing information on morphology and taxonomy of the dinoflagellates. The culture strain of *P. minimum* was a kind gift of Dr S. Yoshimatsu. This work was partly supported by the Sasakawa Scientific Research Grant from The Japan Science Society.

References

Anderson, R. A. (1974). Formation of the bacterial flagellar bundle. In *Swimming and Flying in Nature*, vol. 1 (ed. T. Y. T. Wu, C. J. Brokaw and C. Brennen), pp. 45-56. New York, London: Plenum Press.

Ault, T. R. (2000). Vertical migration by the marine dinoflagellate *Prorocentrum triestinum* miximizes photosynthetic yield. *Oecologia* **125**, 466-475.

Brennen, C. (1974). Locomotion of flagellates with mastigonemes. *J. Mechanochem. Cell Mot.* **3**, 207-217.

Chwang, A. T. and Wu, T. Y. (1971). A note on the helical movement of micro-organisms. *Proc. R. Soc. Lond. B* **178**, 327-346.

Chwang, A. T. and Wu, T. Y. T. (1974). Hydromechanics of flagellar movements. In *Swimming and Flying in Nature*, vol. 1 (ed. T. Y. T. Wu, C. J. Brokaw and C. Brennen), pp. 13-30. New York, London: Plenum Press.

Coakley, C. J. and Holwill, M. E. J. (1972). Propulsion of micro-organisms by three-dimensional flagellar waves. *J. Theor. Biol.* **35**, 525-542.

Crenshaw, H. C. (1996). A new look at locomotion in microorganisms: rotating and translating. *Amer. Zool.* **36**, 608-618.

Eppley, R. W., Holm-Hansen, O. and Strickland, J. D. H. (1968). Some observations on the vertical migration of dinoflagellate. *J. Phycol.* **4**, 333-340.

Franks, P. J. S. (1997). Spatial patterns in dense algal blooms. *Limnol. Oceanogr.* **42**, 1297-1305.

Gaines, G. and Taylor, F. J. R. (1985). Form and function of the dinoflagellate transverse flagellum. *J. Protozool.* **32**, 290-296.

Goldstein, S. F. (1992). Flagellar beat patterns. In *Algal Cell Motility* (ed. M. Melkonian), pp. 99-153. New York: Chapman and Hall.

Gray, J. and Hancock, G. J. (1955). The propulsion of sea-urchin spermatozoa. *J. Exp. Biol.* **32**, 802-814.

Hand, W. G. and Schmidt, J. A. (1975). Phototactic orientation by the marine dinoflagellate *Gyrodinium dorsum* Kofoid. II. Flagellar activity and overall response mechanism. *J. Protozool.* **22**, 494-498.

Higdon, J. J. L. (1979). The hydrodynamics of flagellar propulsion: helical waves. *J. Fluid Mech.* **94**, 331-351.

Holwill, M. E. J. (1966). The motion of *Euglena viridis*: The role of flagella. *J. Exp. Biol.* **44**, 579-588.

Holwill, M. E. J. and Burge, R. E. (1963). A hydrodynamic study of the motility of flagellated bacteria. *Arch. Biochem. Biophys.* **101**, 249-260.

Holwill, M. E. J. and Peters, P. D. (1974). Dynamics of the hispid flagellum of *Ochromonas danica*. *J. Cell Biol.* **62**, 322-328.

Holwill, M. E. J. and Sleigh, M. A. (1967). Propulsion by hispid flagella. *J. Exp. Biol.* **47**, 267-276.

Honsell, G. and Talarico, L. (1985). The importance of flagellar arrangement and insertion in the interpretation of the theca of *Prorocentrum* (Dinophyceae). *Bot. Mar.* **28**, 15-21.

Horstmann, U. (1980). Observations on the peculiar diurnal migrations of a red tide dinophyceae in tropical shallow waters. *J. Phycol.* **16**, 481-485.

Jahn, T. L., Harmon, W. M. and Landman, M. (1963). Mechanisms of locomotion in flagellates. I. *Ceratium*. *J. Protozool.* **10**, 358-363.

Jones, M. S., Le Baron, L. and Pedley, T. J. (1994). Biflagellate gyrotaxis in a shear flow. *J. Fluid Mech.* **284**, 137-158.

Kamykowski, D. (1981). Laboratory experiments on the diurnal vertical migration of marine dinoflagellates through temprature gradients. *Mar. Biol.* **62**, 57-67.

Kamykowski, D., Reed, R. E. and Kirkpatrick, G. J. (1992). Comparison of sinking velocity, swimming velocity, rotation and path characteristics among six marine dinoflagellate species. *Mar. Biol.* **113**, 319-328.

Lamb, H. (1932). *Hydrodynamics*. Sixth edition, pp. 588-614. Cambridge: Cambridge University Press.

Lazier, J. R. N. and Mann, K. H. (1989). Turbulence and the diffusive layers around small organisms. *Deep Sea Res. A* **36**, 1721-1734.

LeBlond, P. H. and Taylor, F. J. R. (1976). The propulsive mechanism of the dinoflagellate transverse flagellum reconsidered. *BioSystems* **8**, 33-39.

Levandowsky, M. and Kaneta, P. J. (1987). Behaviour in dinoflagellates. In *Biology of Dinoflagellates*, vol. 21 (ed. F. J. R. Taylor), pp. 360-397. Oxford: Blackwell Scientific Publications.

Lighthill, J. (1976). Flagellar hydrodynamics. *SIAM Rev.* **18**, 161-230.

MacIntyre, J. G., Cullen, J. J. and Cembella, A. D. (1997). Vertical migration, nutrition and toxicity in the dinoflagellate *Alexandrium tamarense*. *Mar. Ecol. Prog. Ser.* **148**, 201-216.

Miyasaka, I., Nanba, K., Furuya, K. and Nimura, Y. (1998). High-speed video observation of swimming behavior and flagellar motility of *Prorocentrum minimum* (Dinophyceae). *Protoplasma* **204**, 38-46.

Olli, K., Heiskanen Anna, S. and Lohikari, K. (1997). Vertical migration of autotrophic micro-organisms during a vernal bloom at the coastal Baltic Sea: Coexistence through niche separation. *Hydrobiologia* **363**, 179-189.

Olsson, P. and Granéli, E. (1991). Observations on diurnal vertical migration and phased cell divison for three coexisting marine dinoflagellates. *J. Plankt. Res.* **13**, 1313-1324.

Peters, N. (1929). Über Orts- und Geißelbewegung bei marinen Dinoflagellaten. *Arch. Protistenk.* **67**, 291-321.

Sleigh, M. A. (1991). Mechanisms of flagellar propulsion. *Protoplasma* **164**, 45-53.